CHAPTER 8

Budding of Liposomes – Role of Intrinsic Shape of Membrane Constituents

Ales Iglic[1,*] and Veronika Kralj-Iglic[2]

[1]*Laboratory of Applied Physics, Faculty of Electrical Engineering, University of Ljubljana, Trzaska 25, SI-1000 Ljubljana, Slovenia*
[2]*Institute of Biophysics, Faculty of Medicine, University of Ljubljana, Lipiceva 2, SI-1000 Ljubljana, Slovenia*

Contents

Abstract

The budding of phospholipid bilayer membrane is studied theoretically. The description starts from a single-constituent energy that reflects intrinsic shape of the constituent, and uses methods of statistical physics to obtain membrane free energy. The membrane free energy is minimized to yield the equilibrium shape and distribution functions of constituents. It is shown that two mechanisms based on internal degrees of freedom: in-plane orientational ordering of phospholipids in the narrow neck connecting the bud with the mother membrane and clustering of membrane inclusions in the budding region, are complementary mechanisms that promote budding of liposomes.

1. INTRODUCTION

The budding of the bilayer membrane is a process that is vitally important for cells. Accordingly, it is of interest to understand the mechanisms that are involved in the budding. For this, the budding in bilayer membrane vesicles composed of a single phospholipid species have been investigated [1–3]. Changes in the suspension of vesicles, such as changes in temperature and changes in shape of vesicles may in certain conditions induce formation of buds of the

*Corresponding author. Tel.: +386-1-4250-278; Fax: +386-1-4768-850;
E-mail: ales.iglic@fe.uni-lj.si

ADVANCES IN PLANAR LIPID BILAYERS AND LIPOSOMES, VOLUME 4
ISSN 1554-4516 DOI: 10.1016/S1554-4516(06)04008-7

© 2006 Elsevier Inc.
All rights reserved

membrane bilayer [4]. The cell membrane is a multi-component structure, therefore it is of special interest to study the budding of multi-component bilayer membranes. In such membranes, laterally mobile membrane constituents that favor certain membrane curvature, distribute between buds and the mother membrane [5]. Buds may develop into vesicles that alienate from the mother body leading to a loss of the mother membrane material [6]. This is especially significant in vesicles composed of more than one species, since due to the redistribution of the membrane constituents certain substances are accumulated in buds/daughter vesicles [7]. Lateral distribution of membrane constituents can be considered as an internal degree of freedom. The constituents distribute in such a way so as to minimize the membrane free energy [1,8–12]. Besides the lateral distribution of membrane constituents, another internal degree of freedom – lateral distribution of the in-plane orientational ordering of anisotropic constituents – has recently been considered [13–15]. A method has been developed [9,17] starting from the microscopic description of the membrane constituents and applying methods of statistical physics to obtain the membrane free energy. To obtain the equilibrium configuration of the vesicle, the membrane free energy is minimized taking into account the relevant geometrical constraints. The intrinsic properties of membrane constituents and interactions between them are thereby revealed in macroscopic features such as the equilibrium shape of the vesicle. Here, we apply this method while focusing on the effect of the intrinsic shape of the membrane constituents on the internal degrees of freedom, i.e. the equilibrium configuration of the membrane (the orientational ordering and/or the equilibrium membrane shape and the corresponding lateral distribution of constituents). The results presented may contribute to the understanding of abrupt changes in curvature derivatives, the stability of narrow necks that connect buds with the mother membrane, the stability of pear shapes and mechanisms of raft accumulation on the buds.

The description is based on the energy of a single constituent, which depends on the intrinsic shape of the constituents. The introduction of the single-inclusion energy is followed by the statistical mechanical model of the membrane composed of a single species of phospholipid molecules that may undergo in-plane orientational ordering, and a rigorous solution of the variational problem (the minimization of the free energy) yielding equilibrium shapes and the corresponding orientational order distributions of the one-component phospholipid vesicles. Then, the same formalism for the single-inclusion energy and the statistical mechanical model are used to describe spherical budding in the two-component membrane. The solution of the variational problem by a simple parametrical model yields the equilibrium shape and the corresponding lateral distribution of the membrane constituents. The role of the intrinsic shape of the membrane constituents can be recognized throughout the presentation.

2. THE SINGLE-CONSTITUENT ENERGY

Any membrane constituent may be treated as a very small inclusion in a two-dimensional continuum curvature field imposed by other membrane constituents. We assume that the inclusion, due to its structure and local interactions, energetically would prefer a local geometry that is described by the two-intrinsic principal curvatures C_{1m} and C_{2m}. The intrinsic principal curvatures are in general not identical (Fig. 1). If they are identical ($C_{1m} = C_{2m}$), then the in-plane orientation of the inclusion is irrelevant. Such inclusion is called isotropic. If $C_{1m} \neq C_{2m}$ the inclusion is called anisotropic. The orientation of such inclusion is important for its energy. It is assumed that the inclusion will spend on an average more time in the orientation, which is energetically most favorable, than in any other orientation.

If the area and the volume of the vesicle are fixed, the shape cannot attain the curvatures that would equal the intrinsic curvatures in all its points and the energy of the molecules is increased. The energy of a single inclusion derives from the mismatch between the actual membrane shape given by the two principal curvatures C_1 and C_2 and the intrinsic shape given by the intrinsic principal

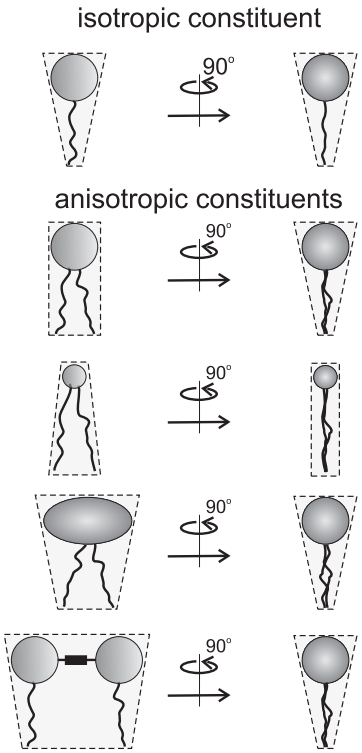

Fig. 1. Schematic representation of different intrinsic shapes of some membrane constituents. Front and side views are shown. Upper: isotropic constituent ($C_{1m} = C_{2m}$), lower: examples of anisotropic constituents ($C_{1m} \neq C_{2m}$).

curvatures C_{1m} and C_{2m} [16,17],

$$E(\omega) = \frac{\xi}{2}(H - H_m)^2 + \frac{\xi + \xi^\star}{4}(\hat{C}^2 - 2\hat{C}\hat{C}_m \cos(2\omega) + \hat{C}_m^2) \tag{1}$$

where ξ and $\xi^\star$ are constants describing the strength of the interaction between the inclusion and the surrounding membrane continuum and in the case of larger multicomponent flexible membrane inclusion also the bending rigidity of the inclusion. $H = (C_1 + C_2)/2$ is the mean curvature of the membrane, $H_m = (C_{1m} + C_{2m})/2$ is the mean curvature of the continuum intrinsic to the inclusion, $\hat{C} = (C_1 - C_2)/2$, $\hat{C}_m = (C_{1m} - C_{2m})/2$ and ω is the orientation of the principal axes of the intrinsic shape relative to the principal axes of the local curvature of the continuum.

It can be seen from equation (1) that the single-inclusion energy attains a minimum when $\cos(2\omega) = 1$, i.e., when the two systems are aligned or mutually rotated by an angle π, while the single-inclusion energy attains a maximum when $\cos(2\omega) = -1$, i.e., when the two systems are mutually rotated by an angle $\pi/2$ or $3\pi/2$. In the first case the single-inclusion energy is

$$E_{\min} = \frac{\xi}{2}(H - H_m)^2 + \frac{\xi + \xi^\star}{4}(D^2 + D_m^2) - \frac{\xi + \xi^\star}{2} D D_m \tag{2}$$

whereas in the second case the single-inclusion energy is

$$E_{\max} = \frac{\xi}{2}(H - H_m)^2 + \frac{\xi + \xi^\star}{4}(D^2 + D_m^2) + \frac{\xi + \xi^\star}{2} D D_m \tag{3}$$

where $D = \left|\hat{C}\right|$ and $D_m = \left|\hat{C}_m\right|$ are the curvature deviator and the intrinsic curvature deviator, respectively. The states $\omega = 0,\pi$ and the states $\pi/2$, $3\pi/2$, respectively, are degenerate so that the ordering is quadrupolar.

3. LIPOSOMES COMPOSED OF A SINGLE KIND OF PHOSPHOLIPID MOLECULES

3.1. The two-state model

A single phospholipid molecule is treated as a very small inclusion in a two-dimensional continuum curvature field imposed by other phospholipid molecules. We assume that the phospholipid molecule, due to its structure and local interactions, energetically would prefer a local geometry that is described by the two principal curvatures C_{1m} and C_{2m}. As the phospholipid molecule is composed of two tails and a headgroup, the intrinsic principal curvatures are not identical (Fig. 1), i.e., the intrinsic shape of the phospholipid molecule is anisotropic [18].

Each monolayer is described separately. The contributions to the free energy of the two monolayers are then summed to obtain the energy of the bilayer membrane.

The monolayer area is divided into small patches that, however, contain a large number of molecules so that the methods of statistical physics can be used. The membrane curvature is taken to be constant over the patch. This curvature field is produced by the molecules themselves, i.e., the molecules pack together in such way as to form the local shape of the membrane. We consider that every phospholipid molecule in the patch is subject to this field. The lattice statistics approach is used, drawing an analogy from the problem of non-interacting magnetic dipoles in an external magnetic field [19], the curvature deviator D taking the role of the external magnetic field.

In the idealized case, we assume a simple model where we have M equivalent molecules in the patch, each existing in one of the two possible states corresponding to the energies $E_{\min}$ and $E_{\max}$, respectively (equations (2) and (3)); N molecules are taken to be in the state with higher energy $E_{\max}$ and $(M-N)$ molecules are taken to be in the state with lower energy $E_{\min}$. The energy of the lipid molecules within the patch in the mean curvature field, divided by kT where k is the Boltzmann constant and T is the temperature, is

$$\frac{E_D}{kT} = N\frac{E_{\max}}{kT} + (M-N)\frac{E_{\min}}{kT} \tag{4}$$

Inserting equations (2) and (3) into equation (4) gives

$$\frac{E_D}{kT} = M\frac{E_{\mathrm{q}}}{kT} - (M/2 - N)d_{\mathrm{eff}} \tag{5}$$

where

$$\frac{E_{\mathrm{q}}}{kT} = \frac{\xi}{2kT}(H - H_m)^2 + \frac{\xi + \xi^\star}{4kT}(D^2 + D_m^2) \tag{6}$$

and

$$d_{\mathrm{eff}} = \frac{(\xi + \xi^\star)D_m D}{kT} \tag{7}$$

We call d_{eff} the effective curvature deviator.

Direct interactions between the membrane constituents are taken into account. Here we assume that the relative orientation of two anisotropic molecules gives rise to a contribution to the direct interaction that is the most important and neglect all other contributions. In describing the direct interaction between the nearest-neighbor molecules, we propose it should be taken into account that the molecules that are oriented in such way that their orientational energy in the mean curvature field is lower, also exhibit more favorable packing. By attaining the shape that is in tune with the local-curvature field, the tails of the favorably oriented molecules come, on the whole, closer together, which gives rise to additional lowering of the energy of the patch due to direct interactions, relative to the situation where the molecules are randomly oriented within the patch. On the

other hand, if we consider that the molecules that are oriented in such way that their orientational energy in the mean curvature field is higher, exhibit less favorable packing, in which the tails are on the whole further apart. This causes a rise of the energy of the interaction between such oriented molecules within the patch with respect to the situation where the molecules are randomly oriented. The effect depends on the local-curvature field, on the intrinsic shape of the molecule and the strength of the interaction. We consider the effect to be proportional to the local effective curvature deviator. The direct interaction of N molecules in the patch that have higher energy $E_{\max}$ with their neighbors is therefore described by a positive contribution [14],

$$\frac{E_N}{kT} = \frac{\tilde{k}}{kT} N d_{\text{eff}} \tag{8}$$

where $\tilde{k}$ is the interaction constant. Accordingly, the direct interaction of $(M-N)$ molecules that have lower energy $E_{\min}$, with their neighbors is described as

$$\frac{E_{M-N}}{kT} = -\frac{\tilde{k}}{kT}(M-N) d_{\text{eff}} \tag{9}$$

The total energy of the patch due to direct interaction E_i/kT is $(E_N/kT + E_{M-N}/kT)/2$, where we divide by 2 as to avoid counting each molecule twice. Therefore,

$$\frac{E_i}{kT} = -\frac{\tilde{k}}{kT}(M/2 - N) d_{\text{eff}} \tag{10}$$

The total energy of the patch E^P is obtained by summing the contribution of the orientation of the molecules according to the local curvature deviator E_D and the contribution of the direct interaction between the molecules within the patch E_i,

$$\frac{E^p}{kT} = \frac{E_D}{kT} + \frac{E_i}{kT} \tag{11}$$

$$\frac{E^p}{kT} = M\frac{E_q}{kT} - \left(1 + \frac{\tilde{k}}{kT}\right)(M/2 - N) d_{\text{eff}} \tag{12}$$

It follows from the above equation that the direct interactions renormalize (enhance) the interaction of the phospholipid molecule with the deviatoric field.

The chosen patch is considered as a system with a constant area A^p and a constant number of molecules M. The system is immersed in a heat bath so that its temperature T is constant. There are two possible energy states for the molecules in the patch. Within the given energy state the molecules are treated as indistinguishable. We assume that the system is in thermodynamic equilibrium and follow the description of a two-orientation model of noninteracting magnetic dipoles [19]. Analogous, if there are N molecules in the state with higher (maximal) energy and $(M-N)$ molecules in the state with lower (minimal) energy, the number of possible arrangements consistent with this N is $M!/N!(M-N)!$, while the

corresponding energy of the system is E^{P}. However, when calculating the partition function, we must consider all possibilities, e.g., N can be any number from 0 to M; $N = 0$ means that all the molecules are in the state with lower energy, $N = 1$ means that one molecule is in the state with higher energy while $M-1$ molecules are in the state with lower energy, etc. The canonical partition function $Q^{\mathrm{p}}(M,T,D)$ of M molecules in the small patch of the membrane is therefore

$$Q^{\mathrm{p}} = \sum_{N=0}^{M} \frac{M!}{N!(M-N)!} \exp\left(-\frac{E^{\mathrm{P}}}{kT}\right) \tag{13}$$

where k is the Boltzmann constant.

Considering equations (2–13) and using the binomial (Newton) formula in summation of the finite series yields

$$Q^{\mathrm{P}} = (2q\cosh(d_{\mathrm{eff}}(1 + \tilde{k}/kT)/2))^{M} \tag{14}$$

where

$$q = \exp\left(-\frac{E_{\mathrm{q}}}{kT}\right) \tag{15}$$

The Helmholtz free energy of the patch is $F^{\mathrm{P}} = -kT \ln Q^{\mathrm{P}}$,

$$\begin{aligned} F^{\mathrm{P}} = {} & \frac{M(3\xi + \xi^{\star})}{4} H^2 - M\xi H H_{\mathrm{m}} - \frac{M(\xi + \xi^{\star})}{4} C_1 C_2 \\ & - MkT \ln\left(2\cosh\left(\frac{d_{\mathrm{eff}}(1 + \frac{\tilde{k}}{kT})}{2}\right)\right) \\ & + \frac{M\xi}{2} H_{\mathrm{m}}^2 + \frac{M(\xi + \xi^{\star})}{4} D_{\mathrm{m}}^2 \end{aligned} \tag{16}$$

where

$$D^2 = H^2 - C_1 C_2 \tag{17}$$

The energy of the membrane bilayer is then obtained by summing the contributions of the all patches in both monolayers,

$$F = \int_{A_{\mathrm{out}}} m_{\mathrm{out}} F^{\mathrm{P}}(C_1, C_2)\, \mathrm{d}A + \int_{A_{\mathrm{in}}} m_{\mathrm{in}} F^{\mathrm{P}}(-C_1, -C_2)\, \mathrm{d}A \tag{18}$$

where m_{out} and m_{in} are the area densities of the lipid molecules in the outer and in the inner monolayer, respectively, while F^{P} is given by equation (16). It is considered that the signs of the principal curvatures in the inner layer are opposite to the signs of the principal curvatures in the outer layer.

We assume that $m_{\mathrm{out}} = m_{\mathrm{in}} = m_0$. Also, in integration, we neglect the difference between the areas of the two monolayers ($A_{\mathrm{out}} = A_{\mathrm{in}} = A_0$), where A is the membrane area. The latter approximation is not valid for strongly curved membranes, but in the system that will be considered in this work, the area

corresponding to strong curvature (i.e. the area of the neck(s)) is small compared to the area of the entire vesicle. It follows from equations (16) and (18) that

$$F = \frac{(3\xi + \xi^\star)}{8} m_0 \int (2H)^2 \, \mathrm{d}A - \frac{(\xi + \xi^\star) m_0}{2} \int C_1 C_2 \, \mathrm{d}A - 2m_0 kT \int \ln \left(2\cosh(d_{\mathrm{eff}}(1 + \frac{\tilde{k}}{kT})/2) \right) \mathrm{d}A \quad (19)$$

The first two terms of the above expression yield the bending energy of a nearly flat thin membrane [20]. In the following, the constant contribution $-2m_0 kTA \ln 2$ that is included in the third term of equation (19) is omitted. Also the second term in equation (19) is not considered further since according to the Gauss–Bonnet theorem it is constant for the closed surfaces that are considered in this work. Therefore, we will further consider the expression for the free energy F [14],

$$F = \frac{(3\xi + \xi^\star)}{8} m_0 \int (2H)^2 \mathrm{d}A - 2m_0 kT \int \ln \cosh(d_{\mathrm{eff}}(1 + \tilde{k}/kT)/2) \, \mathrm{d}A \quad (20)$$

The average number of molecules in each of the energy states represents the local quadrupolar ordering of the molecules. Knowing the canonical partition function of a patch Q^{P} we can calculate the average fraction of the molecules with higher energy within the patch ($E_{\max}$) [14],

$$\frac{\langle N \rangle}{M} = \frac{1}{1 + \mathrm{e}^{d_{\mathrm{eff}}(1 + \tilde{k}/kT)}} \quad (21)$$

while the average fraction of the molecules in the lower energy state $E_{\min}$ is [14],

$$\frac{\langle M - N \rangle}{M} = \frac{1}{1 + \mathrm{e}^{-d_{\mathrm{eff}}(1 + \tilde{k}/kT)}} \quad (22)$$

It can be seen from equations (21) and (22) that at $d_{\mathrm{eff}} = 0$, i.e. when the principal curvatures are equal, both energy states are equally occupied ($\langle N \rangle / M = \langle M - N \rangle / M = 1/2$). The fraction of the number of molecules in the lower energy state increases with increasing d_{eff} to 1, while the fraction of molecules in the higher energy state decreases to 0.

3.2. Global thermodynamic equilibrium

The equilibrium configuration of the system (the equilibrium shape and the corresponding distribution of the quadrupolar ordering) is sought by minimizing the membrane free energy

$$\delta F = 0 \quad (23)$$

under relevant geometrical constraints. We require that the membrane area A

be fixed, that the enclosed volume V be fixed and that the average mean curvature $\langle H \rangle$ be fixed,

$$\int \mathrm{d}A = A, \int \mathrm{d}V = V, \frac{1}{A}\int H\mathrm{d}A = \langle H \rangle \tag{24}$$

For clarity, the above problem is expressed in dimensionless form. We introduce the dimensionless curvatures $c_1 = R_\mathrm{s}C_1, c_2 = R_\mathrm{s}C_2, h = R_\mathrm{s}H, h_m = R_\mathrm{s}H_m$, $\langle h \rangle = R_\mathrm{s}\langle H \rangle, d = R_\mathrm{s}D, d_\mathrm{m} = R_\mathrm{s}D_m$, the relative area $a = A/4\pi R_\mathrm{s}^2 = 1$, the relative volume $v = 3V/4\pi R_\mathrm{s}^3$, the relative area element $\mathrm{d}a = \mathrm{d}A/4\pi R_\mathrm{s}^2$ and the relative volume element $\mathrm{d}v = 3\mathrm{d}V/4\pi R_\mathrm{s}^3$. The normalization unit R_s is the radius of the sphere of the required area A, $R_\mathrm{s} = \sqrt{A/4\pi}$. The free energy of the phospholipid bilayer F (equation (20)) is normalized relative to $(3\xi + \xi^\star)2\pi m_0$,

$$f = w_\mathrm{b} + f_\mathrm{d} \tag{25}$$

where

$$w_\mathrm{b} = \frac{1}{4}\int (c_1 + c_2)^2 \mathrm{d}a \tag{26}$$

$$f_\mathrm{d} = -\kappa \int \ln \cosh(d_\mathrm{eff}(1 + \tilde{k}/kT)/2)\, \mathrm{d}a \tag{27}$$

and

$$\kappa = 4kTR_\mathrm{s}^2/(3\xi + \xi^\star) \tag{28}$$

We consider only axisymmetric shapes. The geometry of the shape is described in terms of the arc length l. We use the coordinates $\rho(l)$ and $z(l)$ where ρ is the perpendicular distance between the symmetry axis and a certain point on the contour and z the position of this point along the symmetry axis. The principal curvatures are

$$c_1 = \frac{\sin\psi}{\rho}, \quad c_2 = \frac{\mathrm{d}\psi}{\mathrm{d}l} \equiv \psi_l \tag{29}$$

where ψ is the angle between the normal to the surface and the symmetry axis. The dimensionless area element is $\mathrm{d}a = \rho \mathrm{d}l/2$ and the dimensionless volume element is $\mathrm{d}v = 3\rho^2 \sin\psi \mathrm{d}l/4$. Using the above coordinates, the dimensionless free energy is

$$f = \int \frac{1}{8}\left(\frac{\sin\psi}{\varrho} + \psi_l\right)^2 \rho\, \mathrm{d}l - \int \frac{\kappa\rho}{2} \ln\, \cosh\left(\vartheta\left(\frac{\sin\psi}{\varrho} - \psi_l\right)\right) \mathrm{d}l \tag{30}$$

where

$$\vartheta = \frac{(\xi + \xi^\star)D_m}{4kTR_s}\left(1 + \frac{\tilde{k}}{kT}\right) \tag{31}$$

while the dimensionless global constraints are

$$\int \frac{1}{2}\rho \, \mathrm{d}l = 1, \quad \int \frac{3}{4}\rho^2 \sin\psi \, \mathrm{d}l = v, \quad \int \frac{1}{4}(\sin\psi + \psi_l \varrho) \, \mathrm{d}l = \langle h \rangle \tag{32}$$

Also, we must consider a local constraint between the chosen coordinates,

$$\frac{\mathrm{d}\rho}{\mathrm{d}l} = \cos\psi \tag{33}$$

A functional is constructed, $G = \int L \, \mathrm{d}l$, where

$$L = \frac{1}{8}\left(\frac{\sin\psi}{\varrho} + \psi_l\right)^2 \rho - \frac{\kappa\rho}{2} \ln\cosh\left(\vartheta\left(\frac{\sin\psi}{\varrho} - \psi_l\right)\right)$$
$$+\lambda_a \frac{\rho}{2} + \lambda_v \frac{3}{4}\rho^2 \sin\psi + \lambda_{\langle h \rangle} \frac{1}{4}\left(\frac{\sin\psi}{\varrho} + \psi_l\right)\rho + \lambda(\rho_l - \cos\psi) \tag{34}$$

λ_a,λ_v and $\lambda_{<h>}$ are the global Lagrange multipliers and λ is the local Lagrange multiplier. The above variational problem is expressed by a system of Lagrange–Euler differential equations,

$$\frac{\partial L}{\partial \rho} - \frac{\mathrm{d}}{\mathrm{d}l}\left(\frac{\partial L}{\partial \rho_l}\right) = 0 \tag{35}$$

$$\frac{\partial L}{\partial \psi} - \frac{\mathrm{d}}{\mathrm{d}l}\left(\frac{\partial L}{\partial \psi_l}\right) = 0 \tag{36}$$

It follows from equations (35) and (34) that [14]

$$\frac{\mathrm{d}\lambda}{\mathrm{d}l} = \frac{1}{8}\left(\frac{\chi^2 - \sin^2\psi}{\rho^2}\right) + \frac{\lambda_a}{2} + \frac{3}{2}\lambda_v \varrho \sin\psi + \frac{1}{4}\lambda_{\langle h \rangle}\frac{\chi}{\rho}$$
$$-\frac{\kappa}{2}\ln\cosh\left(\vartheta\left(\frac{\sin\psi - \chi}{\varrho}\right)\right) + \frac{\kappa\vartheta}{2\rho}\sin\psi \tanh\left(\vartheta\left(\frac{\sin\psi - \chi}{\varrho}\right)\right) \tag{37}$$

while, it follows from equations (36) and (34) that [14]

$$\frac{\mathrm{d}\chi}{\mathrm{d}l} = \frac{A}{B} \tag{38}$$

where

$$B = \left(1 - \frac{2\kappa\vartheta^2}{\cosh^2\left(\vartheta(\sin\psi - \chi)/\varrho\right)}\right) \tag{39}$$

$$A = \frac{\sin\psi\cos\psi}{\rho}\left(1 + \frac{2\kappa\vartheta^2}{\cosh^2\left(\vartheta\left(\frac{\sin\psi - \chi}{\varrho}\right)\right)}\right) - \frac{4\kappa\vartheta^2\chi\cos\psi}{\rho\cosh^2\left(\vartheta\left(\frac{\sin\psi - \chi}{\varrho}\right)\right)}$$

$$+3\lambda_v\varrho^2\cos\psi + 4\lambda\sin\psi - 4\kappa\vartheta\cos\psi\tanh\left(\vartheta\left(\frac{\sin\psi - \chi}{\varrho}\right)\right) \tag{40}$$

and

$$\psi_I = \frac{\chi}{\rho} \tag{41}$$

At the poles $\psi_I = \sin\psi / \rho$.

It follows from equations (38) and (39) that a singularity in $d\chi/dI$ occurs when the denominator (39) becomes equal to 0,

$$1 - \frac{2\kappa\vartheta^2}{\cosh^2(\vartheta(\sin\psi/\rho - \psi_I))} = 0 \tag{42}$$

equation (42) is fulfilled when

$$\frac{\sin\psi}{\rho} - \psi_I = \pm\frac{1}{\vartheta}\ln(\sqrt{2\kappa}\vartheta + \sqrt{2\kappa\vartheta^2 - 1}) \tag{43}$$

i.e. when the curvature deviator attains a certain constant value determined by the constants κ and ϑ. This singularity occurs at sites where the opposing effects of isotropic and deviatoric bending become equal in magnitude, i.e., where the deviatoric effects renormalize the isotropic bending to zero. A geometry is reached where the curvature is so high that the approximate model is no longer valid.

3.3. Solution of the variational problem – the equilibrium shape and orientational distribution

The system of Lagrange–Euler differential equations (37) and (38) is solved numerically. The contour of the axisymmetric equilibrium shape is then given by the two coordinates (ρ,z), where $dz/dI = \sin\psi$. In order to solve the problem numerically, the model constants should be estimated: the interaction constant $\xi^\star$ was for reasons of simplicity taken to be equal to ξ, $\xi = \xi^\star = k_c a_0$, where k_c is the bilayer bending constant and a_0 is the area per phospholipid molecule, $k_c \simeq 20kT$, $a_0 = 60 \times 10^{-20}\text{m}^2$, R_s is 10^{-5} m, $T = 300K$, $D_m = 2 \times 10^8\text{m}^{-1}$, $\vartheta \simeq 1.5 \times 10^{-4}$, $\kappa \simeq 7 \times 10^6$ and $\tilde{k}/kT \simeq 1$ [14]. As $a_0 m_0 = 1$, it follows from above and from the normalization given after equation (24) that the normalization factor of the energies is $(3\xi + \xi^\star)2\pi m_0 = 8\pi k_c$.

Figure 2 shows how the global Lagrange multipliers of an almost globular shape with chosen relative volume and average mean curvature and a chosen constant κ change upon increase of the constant ϑ. It could be expected that the singularity would eventually be reached for high-enough values of ϑ. We call the shape where the singularity first occurs, the critical shape. We were able to overcome the interval of ϑ corresponding to shapes with at least one singularity by extrapolating the solution (the Lagrange multipliers and the boundary conditions) over

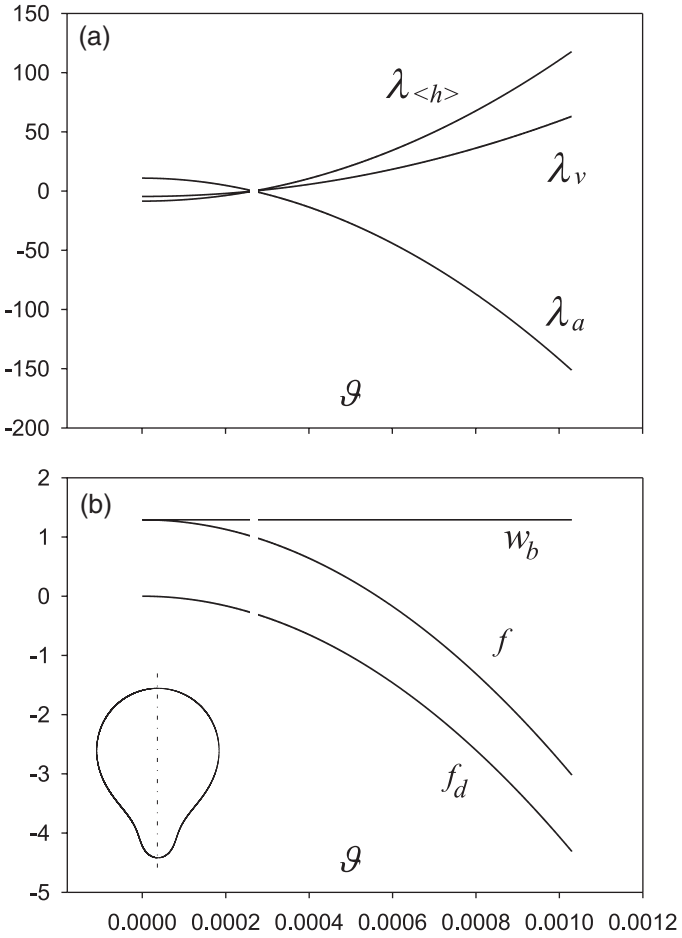

Fig. 2. (a) Lagrange coefficients as a function of the interaction constant ϑ. (b) Bilayer membrane free energy f and the energy contributions: energy of isotropic bending w_b, and contribution of orientational ordering f_d as a function of the interaction constant ϑ. The values of model parameters are $v = 0.95$, $\langle h \rangle = 1.0422$, $\kappa = 7 \times 10^6$ (from Kralj-Iglic *et al* [14]).

this narrow interval. Within this interval we could not solve the variational problem numerically. This is indicated by the gap in the curves (Figs. 2a,b). It can also be seen in Fig. 2a that all the Lagrange multipliers approach zero within this interval.

Figure 2b shows the corresponding dependence of the energy contributions on the value of the constant ϑ. The isotropic bending energy w_b, the deviatoric energy f_d and the sum of these two terms $f = w_b + f_d$ are depicted. It can be seen that close to the interval where the singularity occurs and the Lagrange multipliers approach zero, the dependence of the energy on ϑ indicates no discontinuity. When the interaction constant ϑ is increased over the entire range where the

shapes could be calculated (Fig. 2) the shape change is so minute that the shape appears the same (see inset).

Increasing the constant ϑ in a shape that attains many different values of c_1 and c_2 along the contour (such as the pear-shape with a narrow neck) would first yield a singularity (reach the critical shape) at a single point on the contour (on a ring of axisymmetric shape) in the neck region. It is of interest to study the behavior of the solutions of the variational problem close to the critical shape. Starting with the constants κ and ϑ that are high enough to yield a solution above the interval where the singularity occurs in at least one point on the contour, we approached the critical shape with a somewhat narrower neck by decreasing the constant κ.

Figure 3 shows the contour of the shape and the corresponding fraction of the molecules in the lower energy state, i.e., the ordering of the phospholipid molecules; gray lines correspond to the shape that is more remote to the critical ϑ while black lines correspond to the shape that is closer to the critical ϑ. It can be seen in both cases that the fraction of the molecules in the lower energy state increases in the neck region. In the neck, the curvature deviator is higher and the orientational ordering becomes more pronounced. As the critical ϑ is approached, the maximum of the orientational distribution function becomes narrower and the peak becomes sharper. The neck of the pear-shape becomes shorter and exhibits a more abrupt width change for the shape that is closer to the critical ϑ.

Figure 4 shows the numerator (equation (40)), the denominator (equation (39)) and the derivative $\mathrm{d}\chi/\mathrm{d}l$ along the contour as a function of the symmetry axis of the shapes depicted in Fig. 3. In the shape that is closer to the critical shape (case b) the denominator attains lower absolute values along the whole contour, while it approaches 0 at a certain point in the neck region. Correspondingly, the derivative $\mathrm{d}\chi/\mathrm{d}l$ reaches higher values and changes abruptly in the vicinity of this point forming sharp peaks. In the shape that is more remote to the critical shape (case a), the absolute values of the denominator and of the numerator are higher, while the values of the derivative $\mathrm{d}\chi/\mathrm{d}l$ are lower. The peaks formed by the derivative $\mathrm{d}\chi/\mathrm{d}l$ are milder. The arc length, where the derivative $\mathrm{d}\chi/\mathrm{d}l$ strongly changes diminishes as the critical shape is approached.

Figure 4 shows that the derivative $\mathrm{d}\chi/\mathrm{d}l$ increases when we approach the critical shape, while the numerator and the denominator both decrease over the entire shape. In the point on the contour close to the narrowest width of the neck, the denominator approaches zero. From the numerical results we could not come to a definite conclusion that the regularity condition can be imposed. We could not exclude the possibility that the derivative $\mathrm{d}\chi/\mathrm{d}l$ may in some cases increase beyond any limit. This would mean that the discontinuity in the meridian curvature that is consistent with divergence in $\mathrm{d}\chi/\mathrm{d}l$ corresponds to a finite energy. Changes of the meridian curvature over a minute arc length were recently observed in two-component phospholipid vesicles with added cholesterol, where the two phospholipids were in two different liquid phases (ordered/disordered) [21].

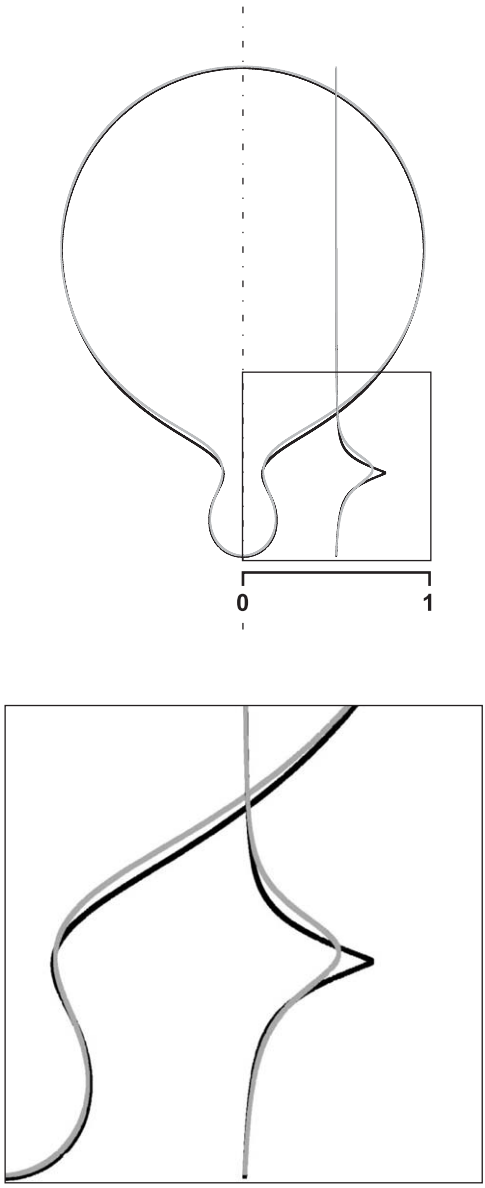

Fig. 3. Two shapes illustrating the approach to the critical shape with singularity in the Euler–Lagrange differential equation and the corresponding orientational distribution functions. The shape that is closer to the critical shape ($\kappa = 1735.5$, black) has a shorter neck and a sharper distribution peak than the shape that is more remote from the critical shape ($\kappa = 2800$, gray). For both shapes $v = 0.95$, $\vartheta = 0.02456$, $\langle h \rangle = 1.11543$ (from Kralj-Iglic *et al* [14]).

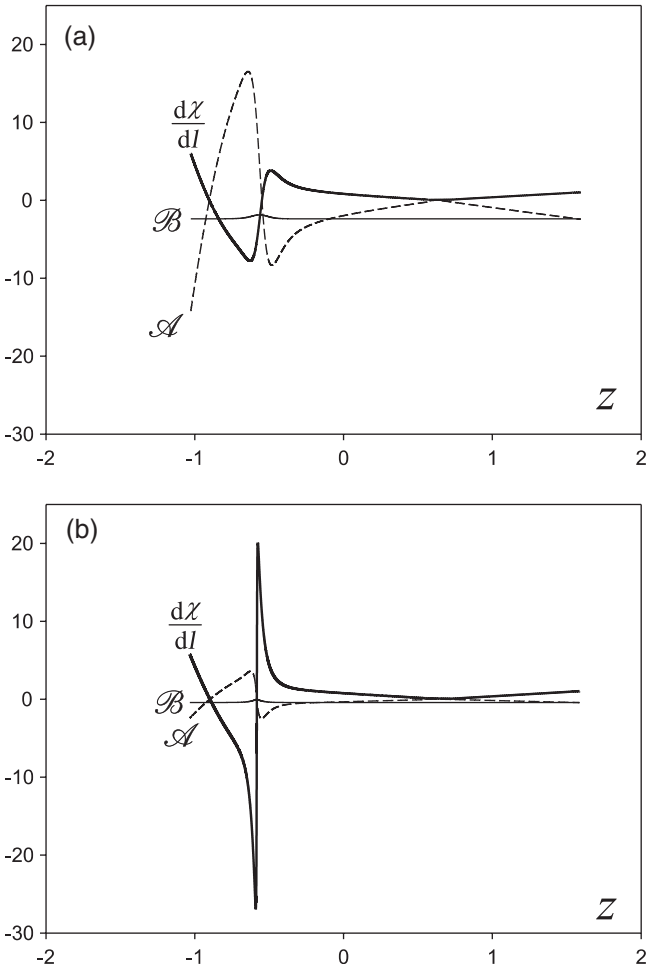

Fig. 4. Approach to the critical shape with singularity in the Lagrange–Euler differential equation. The numerator A, the denominator B and the derivative $d\chi/dl$ are shown for both shapes (a and b, respectively) presented in Fig. 3 (from [14]).

Segregation of the phospholipid was observed whereby an abrupt change in the meridian curvature could be noted in some of the two-photon micrographs. The abrupt changes in curvature appear close to the line where the two phases are in contact, but rather within the disordered phase region. In some shapes, the abrupt change in meridian curvature appears within the disordered phase. It is argued [21] that the shape is determined by the preference of the phospholipid for a certain curvature and by the effects on the edges where the two phases meet; however, the abrupt changes in the curvature within a given phase are not explained.

3.4. Stability of the narrow neck(s)

We studied the sequence of shapes of increasing average mean curvature within the class of pear shapes [2]. It was observed in experiments that the shapes with narrow neck(s) show increased stability [4,17]. For example, in spontaneous transformation of pure palmitoyl oleyl phosphatidylcholine (POPC) vesicles, where the initially long thin protrusion shortens with time, a shape composed of a globular mother vesicle and almost spherical protrusion connected by a narrow neck is attained. Further, the opening of the neck starts; however, the process reverses so that the neck becomes very thin again (Fig. 5). There may be several such oscillations before the neck opens and the vesicle attains its flaccid shape. This indicates an energy minimum of the shape composed of two globular parts connected by a narrow neck. It will be shown below that the orientational ordering of phospholipid molecules in the narrow neck may explain stability of shapes with narrow neck(s).

Figure 6 shows how the free energy of the vesicle changes upon increase of the average mean curvature for a vesicle of a given relative volume $v = 0.95$ and size $R_s = 10^{-5}$ m. Case a corresponds to isotropic bending only, case b corresponds to the quadrupolar ordering of independent molecules ($\tilde{k}/kT = 0$), while case c also considers direct interactions between phospholipid molecules ($\tilde{k}/kT = 1$). The energy of isotropic bending w_b increases along the sequence [22], while the energy of deviatoric bending f_d decreases along the sequence. The behavior of the sum of the two contributions exhibits the difference in the relative rate of change of the two contributions. In case b (if the molecules are considered as independent) the decrease of the energy of the deviatoric bending is not strong enough to overcome the increase of the energy of isotropic bending w_b and f increases with increasing $\langle h \rangle$. In case c (if direct interaction between phospholipid molecules is considered), the increase of the energy of isotropic bending w_b is overcome and the vesicle free energy decreases with increasing $\langle h \rangle$. The rigorous solution of the variational problem (Fig. 6) shows that the effect of quadrupolar ordering on the free energy of the vesicle is also important in shapes, where there are no regions of very high-curvature deviator. Except for in the vicinity of the singularity, the local ordering is low over most of the membrane

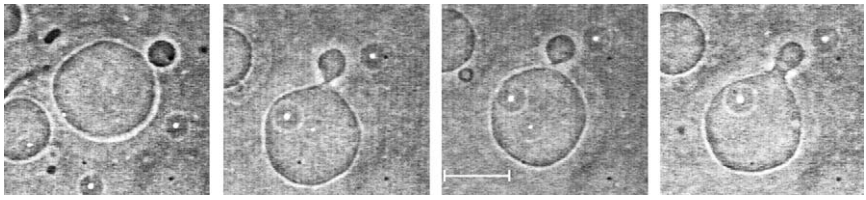

Fig. 5. Oscillations of the neck width before the neck opens and the vesicle attains its flaccid shape indicating that the shape with the narrow neck is energetically favorable, bar = 20 μm (adapted from Iglic and Kralj-Iglic [17]).

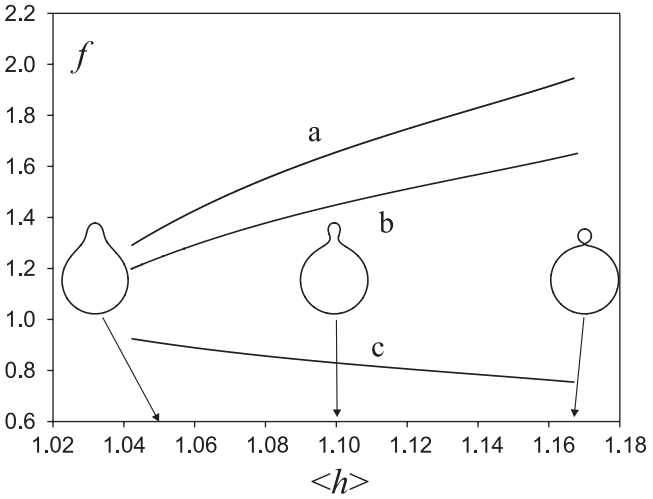

Fig. 6. Bilayer membrane free energy as a function of the average mean curvature of the vesicle with $v = 0.95$; (a) isotropic bending, (b) orientational ordering of independent molecules $\vartheta = 1.5 \times 10^{-4}$,$\kappa = 7 \times 10^{6}$, c: orientational ordering of interacting molecules $\vartheta = 3 \times 10^{-4}$,$\kappa = 7 \times 10^{6}$ (adapted from [14]).

area, while the equilibrium shape could hardly be distinguished from the corresponding shape calculated by minimization of the Helfrich local bending energy. However, as the values of the free energy are considerably affected, the quadrupolar ordering of phospholipid molecules provides a particular interpretation of the trajectories representing the observed processes within the phase diagram of possible shapes. The formation of the neck is energetically favorable for any initiation mechanism. The membrane free energy decreases as the region of increasing curvature deviator increases, while the free energy values remain within the same range (Fig. 6). Similar to exovesiculation (Fig. 4), an energy decrease could also be expected for endovesiculation, by using the same values of the model constants (ϑ and κ). The deviatoric effects could not determine the general direction of the shape change of the globular vesicle, but once the neck(s) start(s) to form, the deviatoric effects provide a mechanism for its stabilization.

3.5. Stability of the pear shape and the ADE model

The mechanism of quadrupolar ordering is complementary to the mechanisms of local and non-local isotropic elasticity of the area-difference-elasticity (ADE) model [3]. The contribution of the non-local isotropic elasticity to the membrane free energy is expressed within the ADE model as [23,3]

$$W_{\mathrm{ADE}} = 2k_{\mathrm{r}}A(\langle H\rangle - H_0)^2 \tag{44}$$

where k_r is the non-local bending constant and H_0 determines the average mean curvature of the membrane under lowest possible stress. The contribution of the non-local isotropic bending normalized by $(3\xi + \xi^{\star})2\pi m_0 = 8\pi k_c$ is

$$w_{ADE} = q(\langle h \rangle - h_0)^2 \tag{45}$$

where $q = k_r / k_c$ and $h_0 = H_0 R_s$.

Within the ADE model, where the free energy consists of the local (26) and non-local (45) isotropic bending, the absolute minimum of the free energy may be by an appropriate choice of the parameters q and h_0 shifted to the limit shape composed of the two spheres connected by an infinitesimal neck. However, a higher value of q than the experimentally estimated one [24] is needed to obtain this effect [3], while the values of h_0 should be taken much larger than any of $\langle h \rangle$ within the sequence of pear shapes, which gives a significant increase in the free energy and concomitant tension within the membrane. It seems unlikely that the vesicle would favor high tension within the membrane as it may develop processes to relax, such as transient pore formation [25,26]. It will be shown below that a decrease of the free energy due to the orientational ordering of phospholipid molecules may complement the non-local isotropic bending in stabilizing pear shapes, including shapes with neck(s).

Figure 7 shows the dependence of the free energy of the vesicle on the average mean curvature $\langle h \rangle$ including the non-local bending of the ADE model for two choices of the parameter h_0 (A: $h_0 = 1.9$, B: $h_0 = 2.1$). Cases a, show the isotropic local and non-local bending (ADE model) while, cases b show the isotropic local and non-local bending and the deviatoric bending due to the quadrupolar ordering of independent molecules ($\tilde{k}/kT = 0$). Since in both cases, A and B, the constant h_0 is larger than any $\langle h \rangle$ of the sequence ($\langle h \rangle < 1.74$), adding a quadratic term of non-local bending to the isotropic local bending increases the membrane free energy (Fig. 7, curves a). If the energy contribution of the deviatoric bending is considered (Fig. 7, curves b), a shallow minimum is obtained for $h_0 = 1.9$ close to the limit shape (at $\langle h \rangle = 1.16$) (A), while for $h_0 = 2.1$ (B) the free energy is decreasing toward the shape with the narrow neck. It can be seen that without considering the deviatoric effect (ADE model alone) the formation of the neck is not favored if the experimental value of the parameter $q = 2$ [24] and the values of h_0 that are comparable to the values of $\langle h \rangle$ within the sequence of the pear shapes are considered. Including the deviatoric effect to the membrane local and non-local isotropic bending renders a minimum close to the shape with the narrow neck. The quadrupolar ordering diminishes the increase of the free energy due to local isotropic bending. Therefore, the sequence becomes more sensitive to the effect of the non-local isotropic bending.

By varying constants ϑ, κ and h_0 within the range that still gives contributions to the free energy that are comparable to the isotropic bending energy, it is also possible to obtain stable pear shapes with a wider neck and deeper minima of the free energy that would exceed the energies of thermal fluctuations. Figure 8

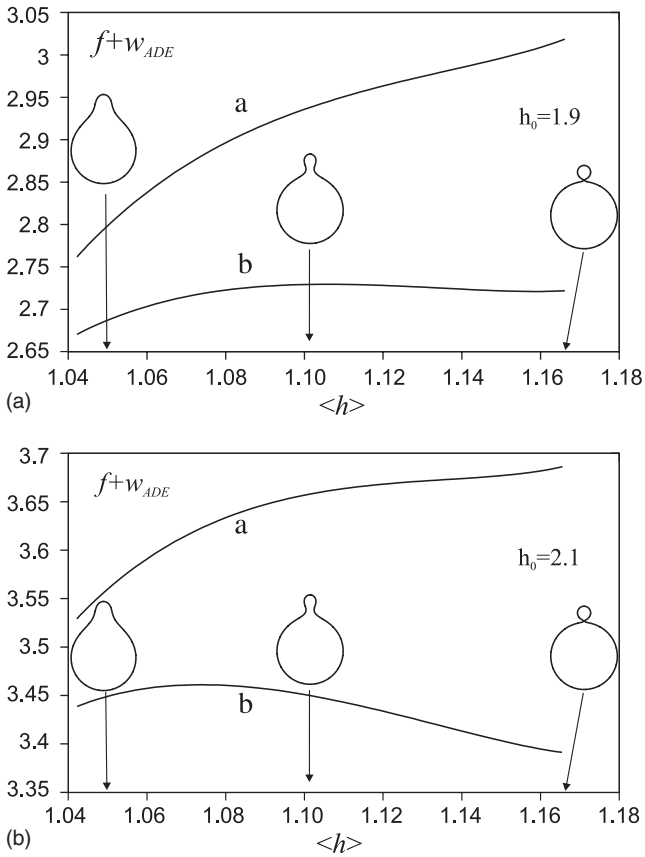

Fig. 7. Bilayer membrane free energy including non-local isotropic bending as a function of the average mean curvature of the vesicle with $v = 0.95$ and $q = 2$. Curves a: local and non-local isotropic bending ($\vartheta = 0$, $\kappa = 0$). Curves b: local and non-local isotropic bending and deviatoric bending due to the orientational ordering ($\vartheta = 1.5 \times 10^{-4}$,$\kappa = 7 \times 10^{6}$).

shows the dependence of the free energy of the vesicle on the average mean curvature including the non-local bending of the ADE model for three choices of the parameter h_0 as given in the figure. It can be seen that it is possible to obtain an absolute minimum also for the shape with a wider neck.

4. SPHERICAL BUDDING IN LIPOSOMES COMPOSED OF TWO KINDS OF MOLECULES

We consider a system composed of phospholipid molecules and membrane-inserted molecules that form together with distorted nearby phospholipid molecules the membrane inclusions [15,22,27]. It is assumed that the inclusions

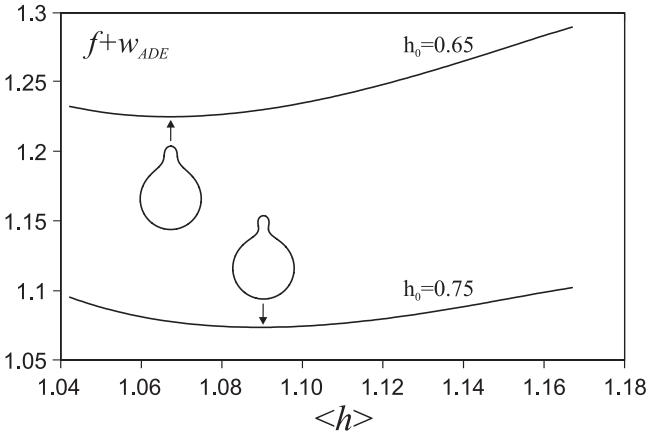

Fig. 8. Bilayer membrane free energy including non-local isotropic bending as a function of the average mean curvature of the vesicle with $v = 0.95$ and $q = 2$ for two choices of the parameter h_0, as given in the figure. The respective shapes, which correspond to the absolute minimum of the free energy within the class of the pear shapes are shown. The values of the model parameters are $\vartheta = 3 \times 10^{-4}$,$\kappa = 7 \times 10^{6}$.

are formed by complexes seeded for example by a protein or a detergent molecule. As such inclusions can be rather large, we take that the energy of a single phospholipid molecule is much smaller than the energy of a single inclusion and will therefore be neglected. For simplicity, inclusions are considered to distribute only in one layer of the bilayer. Due to the lateral mobility of inclusions they accumulate in regions of favorable curvature, while they are depleted from regions of unfavorable curvature [5,22,28]. The influence of the intrinsic shape of the phospholipid molecules on the equilibrium configuration of the system has been described in detail in the previous section, therefore, here we study the effect of the intrinsic shape of larger membrane inclusions seeded, for example, by the intercalated protein or detergent molecule in the membrane.

In order to avoid too high local lateral densities of the inclusions we consider the excluded volume principle, i.e., the finite volume of the membrane components by applying the lattice statistics [19].

As previously, the outer monolayer area is divided into small patches that, however, contain a large number of molecules so the methods of statistical physics can be used. The membrane curvature is taken to be constant over the patch. A lattice is imagined with all its M sites occupied either with a phospholipid molecule or an inclusion. In the chosen patch, there are N inclusions with energy E_N and $(M-N)$ phospholipid molecules with energy 0. The inclusions are taken to be isotropic so that $D_{\mathrm{m}} = 0$. It follows from equation (1)

$$E_N = \frac{\xi}{2}(H - H_{\mathrm{m}})^2 \tag{46}$$

In this case direct interactions between isotropic inclusions are taken into account by using the Bragg–Williams approximation [19]. We assume that the direct interactions [29] are possible only between the inclusions, while there is no direct interaction between the inclusion-phospholipid pairs,

$$W_{\mathrm{ii}} = \bar{N}_{\mathrm{ii}} w \tag{47}$$

where w is the interaction energy of an inclusion–inclusion pair (for $w<0$ the interaction between the inclusions is attractive) and $\bar{N}_{\mathrm{ii}}$ is the average number of nearest–neighbor inclusions,

$$\bar{N}_{\mathrm{ii}} = \frac{1}{2} Nc \frac{N}{M} \tag{48}$$

where, c is the number of nearest neighbors ($c = 4$ for two-dimensional square net. The factor $1/2$ was inserted in order to avoid counting each inclusion-inclusion pair twice. Such direct-interaction energy was used in [8].

The canonical partition function of the inclusions in the patch is

$$Q^{\mathrm{P}} = \exp(-E_N/kT)\exp(-cN^2 w/2MkT)\frac{M!}{N!\,(M-N)!} \tag{49}$$

The Helmholtz free energy of the patch is $F^{\mathrm{P}} = -kT\ln Q^{P}$,

$$F^{\mathrm{P}} = N\frac{\xi}{2}(H - H_{\mathrm{m}})^2 + \frac{cwN^2}{2M} + kTN\ln(N/M) + kT(M-N)\ln((M-N)/M) \tag{50}$$

The membrane free energy is obtained by summing the contributions of all patches in the outer layer. The contribution of the inner layer composed of phospholipid molecules yields a constant contribution since the energy of the phospholipid molecules is taken to be 0, and since all the lattice sites are occupied by equal and indistinguishable molecules. This constant contribution is omitted. Free energy of the vesicle is therefore

$$\begin{aligned} F = & \int_A \frac{\xi m_0}{2}(H - H_{\mathrm{m}})^2 n \,\mathrm{d}A + \int_A \frac{cwm_0}{2} n^2 \mathrm{d}A \\ & + kTm_0 \int_A (n\ln n + (1-n)\ln(1-n))\mathrm{d}A \end{aligned} \tag{51}$$

where $n = N/M$ and $m_0 = M/\mathrm{d}A$.

The equilibrium configuration of the system (the equilibrium shape and the corresponding distribution of the membrane inclusions) is sought by minimizing the free energy

$$\delta F = 0 \tag{52}$$

under relevant geometrical constraints.

We require that there is a fixed number of inclusions in the membrane

$$\frac{1}{A}\int n \ \mathrm{d}A = \bar{n} \tag{53}$$

where, $\bar{n}$ is the average value of n.

For clarity, dimensionless quantities are used. The dimensionless curvatures and the area and volume elements are defined as above (equation (24)). Here, the free energy is normalized relative to kTm_0A,

$$f = \int \frac{\xi}{2kT}(H - H_{\mathrm{m}})^2 n \, \mathrm{d}a + \int \frac{cw}{2kT} n^2 \, \mathrm{d}a + \int (n\ln n + (1-n)\ln(1-n)) \, \mathrm{d}a \tag{54}$$

The dimensionless form of constraint (53) is

$$\int n \ \mathrm{d}a = \bar{n} \tag{55}$$

Here, we will rigorously solve the variational problem only with respect to the distribution of the inclusions n. A functional is constructed, $G = \int L \, \mathrm{d}l$, where

$$L = \frac{\xi}{2kT}(H - H_{\mathrm{m}})^2 n + \frac{cw}{2kT} n^2 + (n\ln n + (1-n)\ln(1-n)) + \lambda_n n \tag{56}$$

and λ_{n} is the global Lagrange multiplier. The relevant Lagrange–Euler differential equation

$$\frac{\partial L}{\partial n} = 0 \tag{57}$$

yields

$$\ln\left[\frac{n}{1-n}\exp\frac{cwn}{kT}\right] = -\lambda - \frac{\xi}{2kT}(H - H_m)^2 \tag{58}$$

For simplicity, we take $\exp(cwn/kT) \approx 1 + cwn/kT$, therefore,

$$\ln\left[\frac{n}{1-n}\left(1 + \frac{cwn}{kT}\right)\right] = -\lambda - \frac{\xi}{2kT}(H - H_m)^2 \tag{59}$$

After rearrangement, equation (59) is solved to obtain

$$n = -\frac{(1 + \mathrm{e}^{-(\lambda+\beta)})kT}{8w} + \frac{(1 + \mathrm{e}^{-(\lambda+\beta)})kT}{8w}\sqrt{1 + \frac{(16w/kT)\mathrm{e}^{-(\lambda+\beta)}}{(1 + \mathrm{e}^{-(\lambda+\beta)})^2}} \tag{60}$$

where, $\beta = \xi n(H - H_{\mathrm{m}})^2/2kT$ and $c = 4$. In the limit of weak interaction (small w) equation (60) transforms into

$$n \cong \frac{\vartheta \exp(-\beta)}{(1 + \vartheta \exp(-\beta))}\left[1 - \frac{4w}{kT}\frac{\vartheta \exp(-\beta)}{(1 + \vartheta \exp(-\beta))^2}\right] \tag{61}$$

where $\vartheta = \exp(-\lambda)$ and $w<0$ for attractive interactions. The parameter ϑ is determined from constraint (53).

To perform minimization of the membrane free energy with respect to the membrane shape, we use a simple parametric model that we consider relevant to discuss a possible physical mechanism explaining the observed curvature-induced sorting of membrane components. We limit our study to buds that have spherical shape. In the model, the membrane is divided into two parts, the planar part (part 1) with the relative area a_1 and the respective fraction of the area covered by the inclusions n_1, and spherically curved part of the membrane (part 2) with the constant mean curvature $H = 1/r$, the relative area a_2 and the respective fraction of the area covered by inclusions equal to n_2. The parameter ϑ is determined numerically from the condition

$$n_1 a_1 + n_2 a_2 = \bar{n} \tag{62}$$

where we take into account

$$a_1 + a_2 = 1 \tag{63}$$

As previously stated, the curved membrane region (region 2) corresponds to the budding (invaginated or evaginated) membrane regions or vesicles.

Figure 9 shows the fraction of the area of the membrane budding (invaginated of evaginated) region covered by inclusions (n_2) as a function of its curvature radius (r) for three values of the intrinsic mean curvature of the inclusions (H_m). It can be seen that for the values of r close to $1/H_m$ the fraction of the membrane curved area occupied by inclusions (n_2) is much larger than $\bar{n}$ even if $w = 0$. This indicates

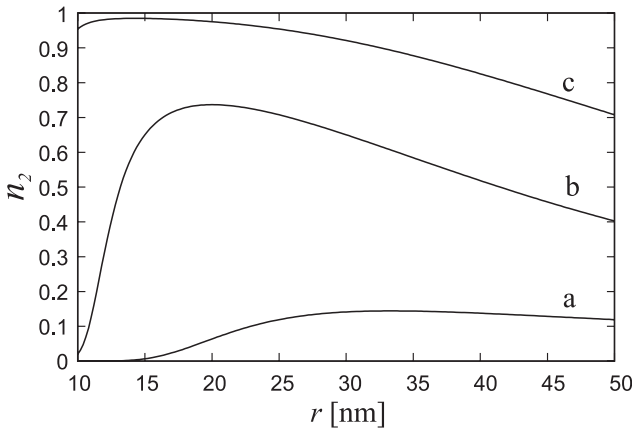

Fig. 9. Fraction of the area of the membrane invaginated or evaginated (budding) region covered by inclusions (n_2) as the function of its curvature radius (r) for three values of the intrinsic mean curvature of the inclusions (H_m): $0.03\,\mathrm{nm}^{-1}$ (a), $0.05\,\mathrm{nm}^{-1}$ (b) and $0.07\,\mathrm{nm}^{-1}$ (c). The values of the other model parameters are: $\bar{n} = 0.02$, $a_2 = 0.02$, $w = 0$ and $\xi = 5000\ kT\,\mathrm{nm}^{-2}$ [28].

the possibility of the curvature-induced clustering of the membrane inclusions in the highly curved membrane regions, i.e., the formation of rafts on membrane invaginations or evaginations and vesicles, due to the preference of inclusions for certain (non-zero) membrane curvature. It can be also seen in Fig. 9 that for high-enough values of the intrinsic mean curvature of the inclusions (H_m) the value of (n_2) approaches unity indicating the possibility of the lateral phase separation of the inclusions for high-enough values of (H_m). For given H_m, the value of r corresponding to maximum of $n_2(r)$ (Fig. 9) also corresponds to minimum of the free energy F, i.e., this value of r is energetically most favorable for given H_m.

Recently, upgradation of the standard model for the cellular membranes [30] with consideration of lateral inhomogeneities of the membrane constituents – rafts [31,32], indicates that budding is important in formation of rafts. Clustering of membrane constituents into larger domains (rafts) in highly curved spherical regions (invaginations) of cell membranes have been observed in biological membranes [33]. It was suggested that small protein–cholesterol membrane complexes (inclusions) may coalesce into larger domains (rafts) [34] upon curvature-induced enrichment of inclusions in highly curved spherical parts of the budding region [35]. The size of membrane inclusions can be very small, comprising just a few molecules (proteins and lipids) [36], but also larger.

For example, it was indicated recently that after generation of ceramidine from sphingomyelin in giant sphingomyelin liposomes, lateral distribution of ceramidine becomes non-homogeneous. Lateral phase separation, i.e., the formation of ceramidine domains, takes place leading to the formation of ceramidine-enriched membrane evaginations/invaginations [5]. It is suggested that the observed lateral segregation of the ceramidine molecules may be a consequence of the interdependence between the local-membrane shape, the local area density of ceramidine molecules and the intrinsic shape of the ceramidine molecules. The role of the direct intermolecular (nearest-neighbor) interactions between ceramidine molecules is also indicated [5].

In the presented theoretical consideration the applied value for the interaction constants ξ is considerably larger than the corresponding value for a single phospholipid molecule [18]. This means that the inclusions considered in Fig. 9 can be membrane proteins, protein–lipid complexes or small clusters of lipid molecules (nanorafts). Therefore they can not be considered as completely rigid bodies as they can adjust their shape to local membrane curvature also by bending. As it is shown in Fig. 9 such inclusions may coalesce into larger rafts upon curvature-induced clustering as indicated in previous studies [34,35].

5. CONCLUSION

In-plane orientational ordering of lipids in the narrow neck connecting the bud with the mother membrane and clustering of membrane inclusions in the budding

region are considered to be complementary driving mechanisms in budding of liposomes (Fig. 10). Both these internal degrees of freedom diminish the membrane free energy. Thereby they counteract the mechanism of isotropic bending and contribute to the relaxation of the membrane. In one-component membrane anisotropic shape of phospholipid molecules (Fig. 1) induces an internal degree of freedom exhibited by in-plane orientational ordering of molecules according to the local membrane curvature. Higher degree of ordering is localized in regions with large difference between the two principal curvatures, e.g., narrow neck(s) (Fig. 10). In multi-component membranes, intrinsic shape of the inclusions induces an internal degree of freedom exhibited by segregation of components (Fig. 9).

Inclusions segregate in the buds (Fig. 10), which fit the intrinsic shape of the inclusions (Fig. 9). Attractive direct interactions between the inclusions promote this effect.

Regions of higher order may present an environment that is favorable for raft formation. Budding with internal degrees of freedom may therefore represent a sorting mechanism that regulates composition of the membrane and lateral distribution of its constituents according to their intrinsic shape and mutual interactions.

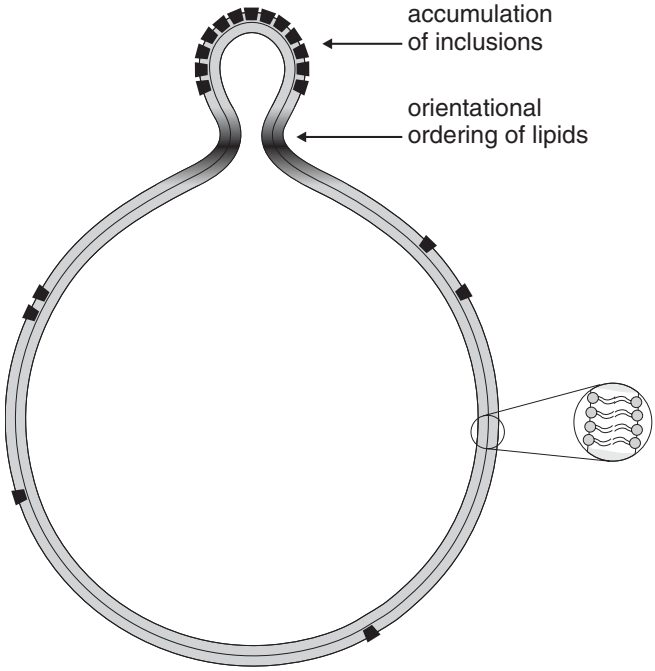

Fig. 10. Schematic presentation of two different complementary driving mechanisms of membrane budding, i.e., clustering of membrane inclusions in the budding region and in-plane orientational ordering of lipids in the narrow neck connecting the bud with the mother membrane.

REFERENCES

[1] E. Sackmann, Membrane bending energy concept of vesicle and cell shapes and shape transitions, FEBS Lett. 346 (1994) 3–16.
[2] R. Lipowsky, The conformation of membranes, Nature 349 (1991) 475–481.
[3] L. Miao, U. Seifert, M. Wortis, H.G. Döbereiner, Budding transitions of fluid-bilayer vesicles: effect of area difference elasticity, Phys. Rev. E 49 (1994) 5389–5407.
[4] J. Käs, E. Sackmann, Shape transitions and shape stability of giant phospholipid vesicles in pure water induced by area – to – volume change, Biophys. J. 60 (1991) 825–844.
[5] J.M. Holopainen, M.I. Angelova, P.K.J. Kinnunen, Vectorial budding of vesicles by asymmetrical enzymatic formation of ceramide in giant liposomes. Biophys. J. 78 (2000) 830–838.
[6] V. Kralj-Iglic, A. Iglic, H. Hägerstrand, P. Peterlin, Stable tubular microexovesicles of the erythrocyte membrane induced by dimeric amphiphiles, Phys. Rev. E 61 (2000) 4230–4234.
[7] H. Hägerstrand, B. Isomaa, Lipid and protein composition of exovesicles released from human erythrocytes following treatment with amphiphiles, Biochim. Biophys. Acta 1190 (1994) 409–415.
[8] V.S. Markin, Lateral organization of membranes and cell shapes. Biophys. J. 36 (1981) 1–19.
[9] V. Kralj-Iglic, S. Svetina, B. Zeks, Shapes of bilayer vesicles with membrane embedded molecules, Eur. Biophys. J. 24 (1996) 311–321.
[10] P.B.S. Kumar, G. Gompper, R. Lipowsky, Budding dynamics of multicomponent membranes, Phys. Rev. Lett. 86 (2001) 3911–3914.
[11] R. Lipowsky, R. Dimova, Domains in membranes and vesicles, J. Phys. Condens. Matter 15 (2003) 531–545.
[12] M. Laradji, P.B.S. Kumar, Dynamics of domain growth in self-assembled fluid vesicles, Phys. Rev. Lett. 93 (2004) 1–4/198105.
[13] J.B. Fournier, Nontopological saddle splay and curvature instabilities from anisotropic membrane constituents, Phys. Rev. Lett. 76 (1996) 4436–4439.
[14] V. Kralj-Iglic, B. Babnik, D.R. Gauger, S. May, A. Iglic, Quadrupolar ordering of phospholipid molecules in narrow necks of phospholipid vesicles, J. Stat. Phys. (2006) (in print).
[15] M. Fosnaric, K. Bohinc, D.R. Gauger, A. Iglic, V. Kralj-Iglic, S. May, The influence of anisotropic membrane inclusions on curvature elastic properties of lipid membranes, J. Chem. Inf. Model. 45 (2005) 1652–1661.
[16] V. Kralj-Iglic, M. Remskar, G. Vidmar, M. Fosnaric, A. Iglic, Deviatoric elasticity as a possible physical mechanism explaining collapse of inorganic micro and nanotubes, Phys. Lett. 296 (2002) 151–155.
[17] A. Iglic, V. Kralj-Iglic, Effect of anisotropic properties of membrane constituents on stable shape of membrane bilayer structure, in: H. Ti Tien, A. Ottova-Leitmannova (Eds.), Planar Lipid Bilayers (BLMs) and Their Applications, Elsevier, Amsterdam, London, 2003, pp. 143–172.
[18] V. Kralj-Iglic, A. Iglic, G. Gomiscek, F. Sevsek, V. Arrigler, H. Hägerstrand, Microtubes and nanotubes of a phospholipid bilayer membrane, J. Phys. A: Math. Gen. 35 (2002) 1533–1549.
[19] T.L. Hill, An Introduction to Statistical Thermodynamics, General Publishing Company, Toronto, 1986, pp. 209–211..
[20] W. Helfrich, Elastic properties of lipid bilayers – theory and possible experiments, Z. Naturforsch. 28c (1973) 693–703.
[21] T. Baumgart, S.T. Hess, W.W. Webb, Imaging coexisting fluid domains in biomembrane models coupling curvature and line tension, Nature 425 (2003) 821–824.
[22] V. Kralj-Iglic, V. Heinrich, S. Svetina, B. Zeks, Free energy of closed membrane with anisotropic inclusions, Eur. Phys. J. B 10 (1999) 5–8.

[23] E.A. Evans, R. Skalak, Mechanics and Thermodynamics of Biomembranes, CRC Press, Boca Raton, FL, 1980.
[24] W.C. Hwang, R.A. Waugh, Energy of dissociation of lipid bilayer from the membrane skeleton of red blood cells, Biophys. J. 72 (1997) 2669–2678.
[25] J.M. Holopainen, M.I. Angelova, Söderlund, P.J. Kinnunen, Macroscopic consequences of the action of phospholipase C on giant unilamellar liposomes, Biophys. J. 83 (2002) 932–943.
[26] R.M. Raphael, R.E. Waugh, Accelerated interleaflet transport of phosphatidylcholine molecules in membranes under deformation, Biophys. J. 71 (1996) 1374–1388.
[27] S. Marcelja, Chain ordering in liquid crystals II. Structure of bilayer membranes, Biophys. Biochim. Acta 367 (1974) 165–176.
[28] A. Iglic, M. Fosnaric, H. Hägerstrand, V. Kralj-Iglic, Coupling between vesicle shape and the non-homogeneous lateral distribution of membrane constituents in Golgi bodies, FEBS Lett. 574/1–3 (2004) 9–12.
[29] K. Bohinc, V. Kralj-Iglic, S. May, Interaction between two cylindrical inclusions in a symmetric lipid bilayer, J. Chem. Phys. 119 (2003) 7435–7444.
[30] S.J. Singer, G.L. Nicholson, The fluid mosaic model of the structure of cell membranes, Science 175 (1972) 720–731.
[31] D.A. Brown, E. London, Structure and origin of ordered lipid domains in biological membranes, J. Membr. Biol. 164 (1998) 103–114.
[32] K. Simons, E. Ikonen, Functional rafts in cell membranes, Nature 387 (1997) 569–572.
[33] T. Harder, K. Simons, Caveolae, DIGs, and the dynmics of sphingolipid-cholesterol microdomains, Curr. Opin. Cell. Biol. 9 (1997) 534–542.
[34] J.C. Holthius, G. van Meer, K. Huitema, Lipid microdomains, lipid translocation and the organization of intracellular membrane transport (review), Mol. Membr. Biol. 20 (2003) 231–241.
[35] C. Thiele, M.J. Hannah F. Fahrenholz, W.B. Huttner, Cholesterol binds to synaptophysin and is required for biogenesis of synaptic vesicles, Nat. Cell. Biol. 2 (1999) 42–49.
[36] K. Jacobson, C. Dietrich, Looking at lipid raft? Trends Cell Biol. 9 (1999) 87–91.